Journal of Materials Chemistry A

Accepted Manuscript

ROYAL SOCIETY OF CHEMISTRY

www.rsc.org/materialsA

Cite this: DOI: 10.1039/c0xx00000x

www.rsc.org/xxxxxx

ARTICLE TYPE

Sheet-like $MoSe_2$/C composites with enhanced Li-ion storage properties

Yuan Liu,[a] Minqiang Zhu[a] and Di Chen[b]*

Received (in XXX, XXX) Xth XXXXXXXXX 200X, Accepted Xth XXXXXXXXX 200X
DOI: 10.1039/b000000x

Carbon composited transition-metal dichalcogenides have demonstrated favourable applications in lithium ion batteries. Herein, sheet-like $MoSe_2$/C composites were successfully synthesized using $Na_2MoO_4{\cdot}2H_2O$, Se powder and glucose as source materials through a simple hydrothermal method and subsequently annealing treatment. The as-synthesized sheet-like $MoSe_2$/C composites were characterized by XRD, FSEM, FTEM, and XPS, respectively. When fabricated into lithium-ion batteries, the composites exhibit improved Li storage performance than pure $MoSe_2$ electrode, including good cycling stabilities and high rate capacity. After 50 cycles, a reversible specific capacity of about 576.7 $mAhg^{-1}$ at the current density of 100 mAg^{-1} was still achieved for the sheet-like composites electrode.

Introduction

Nowadays, rechargeable lithium ion batteries have been widely used to provide power for many portable electronics like mobile phones, notebooks, laptops and many other consumer products because of their high energy density, long cycle life and environmentally friendliness.[1-5] Compared to traditional energy storage devices, such as nickel metal hydride, alkaline and lead–acid batteries, LIBs with higher volumetric and gravimetric energy density are more suitable candidates for potential green applications in electric vehicles (EVs) and hybrid electric vehicles (HEVs).[6,7] However, the commercially used anode materials of LIBs, graphite, with a theoretical specific capacity of only 372$mAhg^{-1}$ and relatively poor rate capability cannot meet the increasing demand in EVs and HEVs.[8-10] Therefore, developing new kind of alternative anode materials to satisfy the demands of future high-performance battery units is the urgent task.

Different from bulk materials, two dimensional nanostructures have shortened path length for Li^+ diffusion and large exposed surface area offering more Li^+ insertion channels, which play important roles in enhancing the performance of Li-ion batteries.[11] For example, Zhu et al. successfully synthesized ultrathin SnO_2 nanosheets through a microwave-assisted method using tin dichloride as the precursor. The as-synthesized SnO_2 nanosheets exhibit a high reversible capacity of 757.6mAh g^{-1} at the rate of 200 mAg^{-1}.[12] Ultrathin silicon nanosheets were synthesized by Yan's group using GO nanosheets as sacrificial hard template. When evaluated as anode for lithium-ion batteries at a current density of 420mAg^{-1}, the ultrathin Si nanosheets electrode still achieved a reversible discharge capacity of 600 $mAhg^{-1}$ after 100 cycles, much higher than silicon nanoparticles.[13] Moreover, Wu and co-workers synthesized sheet-like Fe_2O_3 from a simple coprecipitation technique at room temperature and obtained high rate capacity (1327$mAhg^{-1}$ at 1C, 1215$mAhg^{-1}$ at 3C), when assembled into Li-ion batteries.[14]

Transition-metal dichalcogenides MX_2 (M =Mo, W; X = S, Se) with layer structure like graphene have received great attention in recent years.[9,15] In these compounds, atoms within layers are bound by strong covalent bonds (X-M-X), while the individual layer is bound by weak van der-Waals interactions, forming a sandwich-like structure,[16-20] which is beneficial for the intercalation/deintercalation of Li ions. In the past decades, great attention has been paid to molybdenum sulfide (MoS_2) because of its high theoretical specific capacity and relatively high stability.[21-25] With the same layer structure, it can be concluded that $MoSe_2$ might be a good choice for energy storage devices. Previously, some reports have investigated the synthesis and the applications of $MoSe_2$ in field-effect transistors,[26-28] catalyst[29,30] and Li-ion batteries,[31] etc.

In this work, we developed a facile process to grow sheet-like $MoSe_2$/C composites by a simple solution-phase method. Encouragingly, the as-synthesized $MoSe_2$/C composites exhibit outstanding electrochemical lithium-storage performance, e.g. good rate capability, long cycle life and capacity retention owing to the layer structure, the high surface area and improved electrical conductivity.

Experimental

Materials synthesis

All the chemicals were used as received without further purification. The synthetic process is referred to previous report with some modified experimental conditions.[32] In a typical synthetic process, 1.78 g glucose was first dispersed in 50 ml distilled water under constant stirring to form a clear solution, then 2 mmol $Na_2MoO_4{\cdot}2H_2O$ (99.99%) was dissolved into the solution. In a separate flask, 4 mmol Se powder was dissolved in 10 ml hydrazine hydrate ($N_2H_4H_2O$, 85%) in the open air. After stirring for about 1 hour, the Se solution was slowly added into Na_2MoO_4 solution at room temperature and the mixture solution gives an orange-red color. Then, the mixture was transferred into

the Teflon-lined autoclave and heated in an electric oven at 220°C for 12 h. After cooling to room temperature naturally, the black precipitates were collected by vacuum filtration, washed with deionized water and ethanol for several times, and then dried in a vacuum oven at 80 °C for 12 h. Subsequently, the obtained samples were annealed in a conventional tube furnace at 500 °C for 5 h in high purity nitrogen atmosphere flowing at 200 sccm to get rid of the redundant Se powder. To make a comparison, pure $MoSe_2$ was also prepared from the similar process with the absence of glucose.

Materials characterization

The X-ray diffraction (XRD) patterns were tested using X-ray diffractometer (X'Pert PRO, PANalytical B.V., The Netherlands) with Cu Ka radiation (λ = 0.154 nm). X-ray photoelectron spectrometer was performed on a VG Multi-lab 2000 system with a monochromatic Al Ka X-ray source. TGA analysis was performed on PerkinElmer Diamond (Pyris1 TGA) apparatus at a heating rate of 10 °C/min in air. The morphologies and structure of the as-synthesized products were characterized by field emission scanning electron microscope (Nova NanoSEM 450, FEI, The Netherlands) and field Emission Transmission Electron Microscopy (Tecnai G2 F30, FEI, The Netherlands) coupled with an energy dispersive X-ray spectrometer (EDX).

Electrochemical measurements

The electrochemical properties of the as-synthesized samples were investigated in a two-electrode coin cell (CR2032) configuration assembled in an argon-filled glove box. Lithium metal was served as the counter electrode, and a polypropylene film (Celgard-2300) was used as the separator. The electrolyte was 1.0 M LiPF6 solution with a mixture of ethylene carbonate and diethyl-carbonate (EC/DMC, 1:1 in volume). The working electrodes were prepared by coating the slurry consisting of 70wt.% active materials, 20wt.% acetylene black and 10wt.% polyvinylidene fluoride (PVDF) dispersed in N-methyl-2-pyrrolidinone (NMP) onto a copper foil and dried at 80 °C for about 24 hours. Then, it was cut into round pieces with a diameter of 8 mm. Galvanostatic charging and discharging tests were conducted using a battery testing system (Land, China) at 100 mA g^{-1} with the potential ranging from 5 mV to 3V. Cyclic voltammetry (CV) at a scan rate of 0.1 mVs^{-1} and electrochemical impedance spectrometry in the frequency range of 100 kHz to 10 mHz were measured on an electrochemical workstation (CHI 760D, CH Instruments Inc, Shanghai) at room temperature.

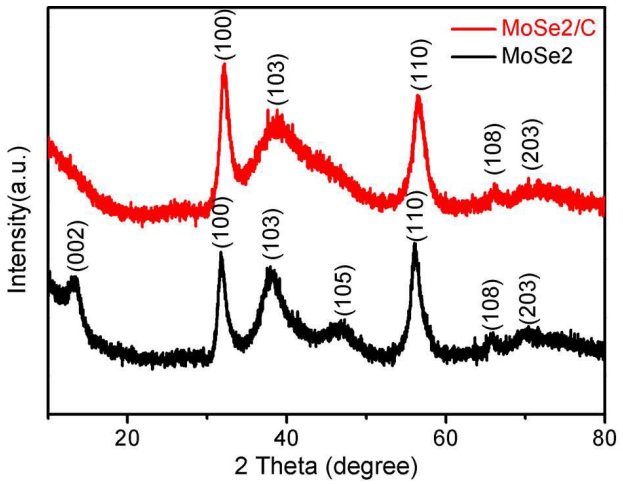

Fig.1 XRD patterns of pure $MoSe_2$ and sheet-like $MoSe_2$/C composites.

Results and discussion

Sheet-like $MoSe_2$/C composites were prepared from the facile hydrothermal and subequently heat-treated processes. The composition and purity of samples were first characterized by XRD. As shown in Fig. 1, all the diffraction peaks can be indexed to 2H-$MoSe_2$ phase (JCPDS Card No. 77-1715). In the pattern of $MoSe_2$/C composites, two peaks located at 2θ = 13.7° and 47.5° corresponding to (002) and (105) planes disappeared compared to that of pure $MoSe_2$, which can be attributed to the carbon component formed by carbonization of glucose decreased the stacking of the $MoSe_2$ layers. XRD patterns of $MoSe_2$ with different carbon content were shown in Fig. S1. Obviously, with the increasing carbon content, the intensity of (002) plane diffraction peak of $MoSe_2$ became weaker till disappeared.

The morphologies of the as-synthesized $MoSe_2$/C composites were first characterized by field-emission scanning electron microscopy (FSEM) and field emission transmission electron microscopy (FTEM). Fig. 2 shows SEM and TEM images of the as-synthesized sheet-like $MoSe_2$/C composites. As shown in Fig. 2a, the $MoSe_2$/C composites with better dispersibility are typically sheet-like structure assembled by many ultrathin nanosheets, which is different from the aggregated structure of pure $MoSe_2$ products (Fig. 4a), indicating that the presence of glucose in the system has great influence on the morphologies of products in our experiment. Fig. 2b-2d further show TEM images of sheet-like $MoSe_2$/C composites. Clearly, $MoSe_2$/C composites with curling sheet-like structure are thinner than pure $MoSe_2$ samples (Fig.4b). HRTEM image of the composites in Fig. 2e shows the lattice fringe spacing of approximately 0.289 nm, corresponding to (100) plane of $MoSe_2$. Moreover, the lattice fringe of $MoSe_2$/C is not as clear as that of pure $MoSe_2$ (Fig. 4d), The stacking of pure $MoSe_2$ layers observed from Fig.4c was relatively more obvious than that of $MoSe_2$/C composites (Fig. 2c), which is correspongding to our XRD annlysis well.

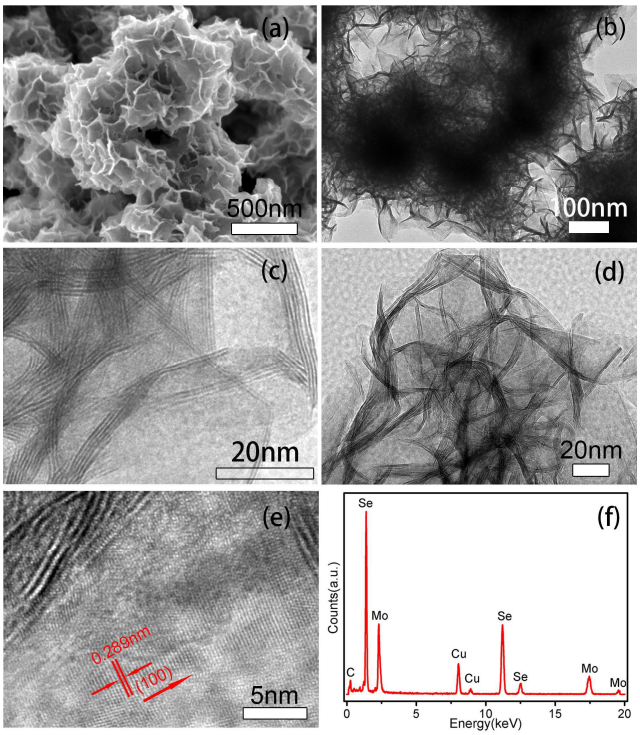

Fig. 2 SEM (a), TEM (b, c, d), HRTEM images (e) and EDS (f) of the as-synthesized sheet-like $MoSe_2$/C composites.

To further determine the composition of sheet-like $MoSe_2$/C composites, energy dispersive X-ray spectroscopy (EDS) were carried out as shown in Fig. 2f. The obtained spectrum suggests the existence of three elements C, Mo, Se, respectively, and the Cu signal in the spectrum arises from the Cu grid. Based on the EDS results, the atomic ratio of Se and Mo is 2.08:1, very close to the theoretical value of $MoSe_2$. In order to determine the elements dispersion and further determine the existence of carbon in sheet-like $MoSe_2$/C composites, the corresponding EDAX mappings of C, Mo, Se are shown in Fig. 3, revealing the uniform dispersion of carbon in $MoSe_2$/C composties. Furthermore, TGA measurements were performed to test the content of carbon in the composites. As shown in Fig. S2, with the increase of temperature, the weight of composites changed largely. The weight increased until the temperature up to 350 ^{o}C, which can be attributed to the formation of SeO_2 and MoO_3 during the oxidation of $MoSe_2$ sample. When the temperature decreased to 550 ^{o}C, the weight lost due to the gasification of SeO_2. At last, $MoSe_2$ converted into MoO_3 and the amorphous carbon converted into CO_2. Thus, the content of carbon in the as-synthesized $MoSe_2$/C composites is about 10 wt.% based on the TGA results. Considering that the carbon content is a bit lower than expected, we also performed a comparative reaction that only glucose and hydrazine hydrate without $Na_2MoO_4{\cdot}2H_2O$ and Se powder are in the solution. When the reaction finished, no carbon products were obtained from this similar process. It can be concluded that the hydrazine hydrate in this hydrothermal procedure hinders the carbonization of glucose.

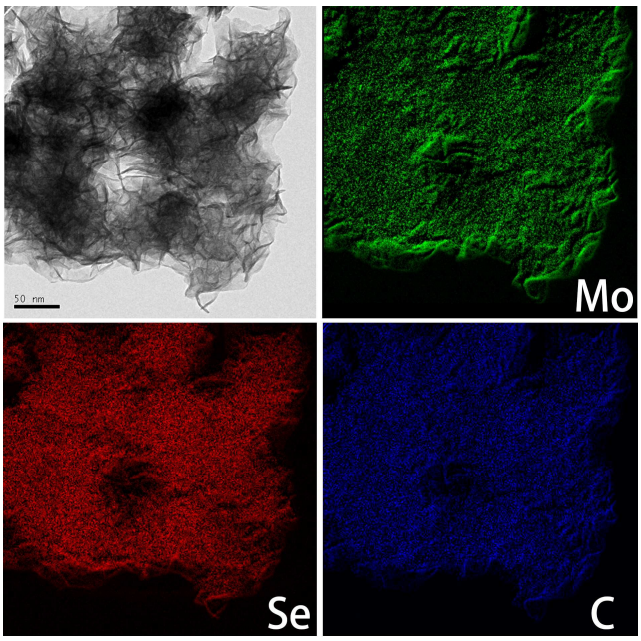

Fig. 3 TEM image and corresponding EDAX mapping of C, Mo, Se in the $MoSe_2$/C composites.

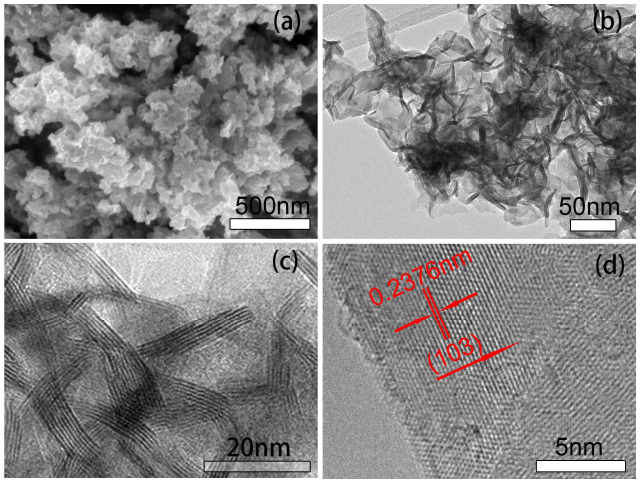

Fig. 4 SEM (a), TEM (b, c) and HRTEM images (d) of the as-synthesized pure $MoSe_2$.

The morphology and microstructure of pure $MoSe_2$ prepared from similar process were also characterized in this work. Fig. 4a shows the FSEM image of pure $MoSe_2$, in which many irregular nanosheets aggregated together each other. Fig. 4b and 4c display the TEM images of the products. Obviously, $MoSe_2$ products show typical layer structure. Fig. 4d shows the HRTEM of the pure $MoSe_2$, The fringes are separated by about 0.2376 nm, corresponding to the interplanar distance for (103) plane very well.

To analyze the chemical composition on the surface and the valence states of sheet-like $MoSe_2$/C composites, X-ray photoelectron spectroscopy (XPS) measurements were carried out in the region of 0-1200 eV. The survey spectrum of composites (Fig. 5a) indictates the presence of three elements. Fig. 5b further shows the C 1s spectrum, which could be deconvoluted into three peaks, the carbon in C-C at 284.6 eV,[33,34] the carbon in C-OH at 286.2 eV and the carbon in C-Mo at 282.5 eV, respectively.[35] The

high resolution Mo 3d spectrum of the composites exhibits two peaks at 229 eV and 232.1eV (Fig. 5c), corresponding to the Mo $3d_{5/2}$ and $3d_{3/2}$ spin orbit peaks of $MoSe_2$ confirming the exitance of Mo IV state. The 3d peak of Se element is split into well-defined two peaks at 54.5 eV and 55.4 eV, corresponding to the Se $3d_{5/2}$ and Se $3d_{3/2}$ characterize peaks, further illustrating the products are $MoSe_2$/C.[32,36]

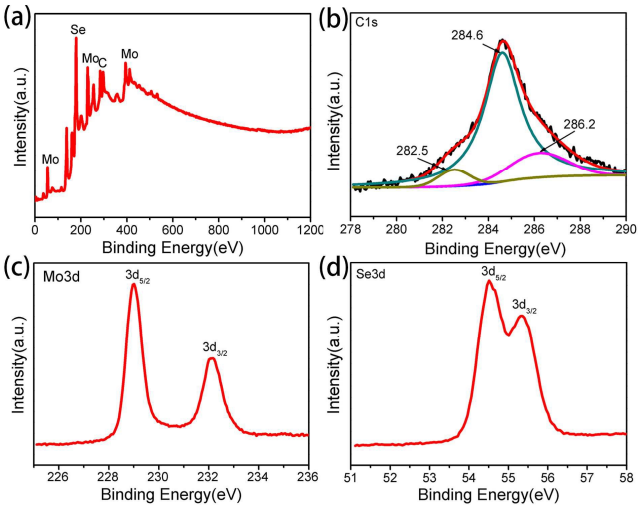

Fig. 5 XPS spectra for the as-synthesized $MoSe_2$/C composites: a) survey spectrum and high resolution spectrum of b) C 1s, c) Mo 3d, d) Se 3d.

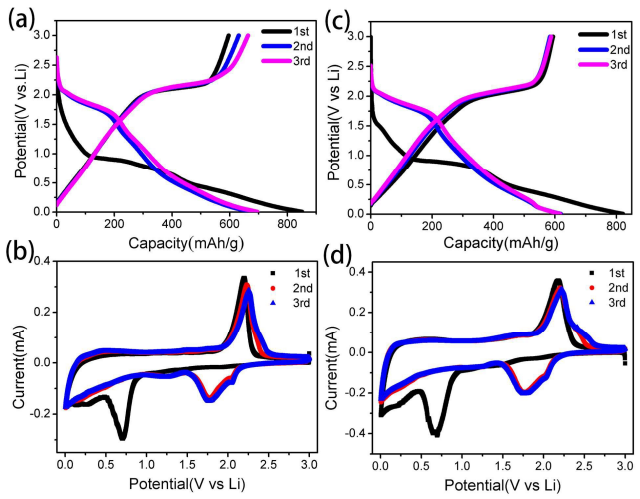

Fig. 6 First three CV curves and charge/discharge profiles of pure $MoSe_2$ (a, b) and sheet-like $MoSe_2$/C composites (c, d).

The as-synthesized sheet-like $MoSe_2$/C composites were assembled into coin cell and evaluated for the lithium storage performance. To make a comparison, pure $MoSe_2$ products were also performed for the same tests. Although the related lithium storage mechanism of $MoSe_2$ electorde is still not clear, similar lithium intercalation/deintercalation processes can be refered to those happened in MoS_2 electorde due to their same layer structure. Fig. 6a and 6c show the first three cyclic voltammetry (CV) profiles of the composites and pure samples, respectively. In the first cathodic porcess, two reduction peaks appear at approximate 0.7 V and 0.25V, corresponding well with Li intercalation into layered $MoSe_2$ electorde and the conversion into Mo metal as well as the formation of SEI layer at the interface of the electrolyte and the electrode, respectively.[15,37] While in the first anodic process, an obvious peak appears at approximately 2.2 V may be attributed to the oxidation reaction of Mo to $MoSe_2$. In the subsequent process, the shape of CV curves and the oxidation/reduction peaks still remain constant illustrating the good stability of the electrochemial process. Fig. 6b and 6d further show the galvanostatic charge/discharge profiles of both samples in the voltage range of 5mV–3V (vs.Li^+/Li) at a current density of 100 mAg^{-1}. Upon the initial discharge curve, two potential plateaus at 1.8V and 0.3V can be observed which are in agreement with the CV curves. Calculated from the charge/discharge curves, sheet-like $MoSe_2$/C composites deliverd the initial discharge and charge capacity of 821.7$mAhg^{-1}$ and 593.7mAh g^{-1}, and pure $MoSe_2$ delivered the initial discharge and charge specific capacities of 851.1 mAh g^{-1} and 595.6 mAh g^{-1}, respectively.

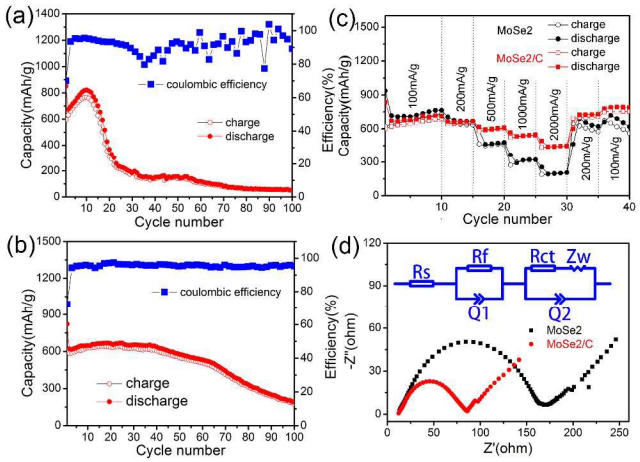

Fig. 7 Cycling performance and coulombic efficiency of pure $MoSe_2$ (a) and sheet-like $MoSe_2$/C composites (b), rate performances (c) and EIS (d) of pure $MoSe_2$ and sheet-like $MoSe_2$/C composites.

Fig. 7a and 7b show the cycling performance of sheet-like $MoSe_2$/C composites and pure $MoSe_2$ at a current density of 100mAg^{-1} for 100 cycles. Clearly, after 50 cycles, sheet-like $MoSe_2$/C composites exhibit a superior reversible discharge capacity of 576.7 mAh g^{-1} (93% capacity retention) at the current density of 100 mA g^{-1}. During the cycling process, the Moe_2/C composites also display enhanced cycling stability and better coulombic efficiency than pure $MoSe_2$ electrodes. To further investigate the electrochemical performance of sheet-like $MoSe_2$/C composites and pure $MoSe_2$ electrode, the rate capability of both samples were further compared. As shown in Fig. 7c, with increased rate current, the sheet-like $MoSe_2$/C composites exhibht lower capacity decrease compared to pure $MoSe_2$ electrode. For example, when the current density increases to 1000 mAg^{-1}, the specific capacity of sheet-like $MoSe_2$/C composites still remains 540 mAh g^{-1}, which is much larger than that of pure $MoSe_2$. Remarkably, the reversible capacity is also retained about 450 mAg^{-1} even with the rate up to 2000 mAg^{-1}. When the current density returned back to 100 mAg^{-1}, the capacity of the composits is recoverd without capacity decreasing.

To gain insight into the reason that sheet-like $MoSe_2$/C composites possess such better electrochemical peformances for lithium storage, the electrochemcical impedance spectroscopy (EIS) before and after 5 cycles were measured and results are shown in Fig. 7d and Fig. S3, respectively, which can help us understand the kinetics of the electrochemcial reaction between the electrode and the electrolyte.[38] Clearly, the diameter of the semicircle for sheet-like $MoSe_2$/C composites in the high-medium frequency region is smaller compared with that of pure $MoSe_2$ electrode, indicating that the $MoSe_2$/C composites possess lower contact and charge-transfer resistances. To further evaluate the electrochemcial performance of two electrodes, the equivalent circuit model is also shown in Fig. 7d inset to illustrate the performance of the composite electrodes.[38,39] Typically, Rs represents the electrolyte resistance corresponding to the intercept of the semicircle at high frequency range. Rf and Q1 are the SEI layer resistance and the constant phase element (CPE), respectively, corresponding to the semicircle at high frequency range. Rct and Q2 are the charge transfer resistance and related double layer capacitor, respectively, corresponding the semicircle in high-middle frequency region. And Zw is Warburg impedance corresponding to the straight line in low frequency range related to the lithium-diffusion process. The fitting results are summarized in Table S1. It can be seen that the SEI film resistance Rf and charge-transfer resistance Rct of the $MoSe_2$/C electrode before and after 5 cycles are 71.58Ω, 105.4Ω and 128.6Ω, 224.3Ω, respectively, which are significantly lower than those of the pure $MoSe_2$. Thus, it can be concluded that the presence of amorphous carbon in the composites can increase the electric conductivity, which is agree with the previous reports very well.[40] It also should be noted that the SEI layer resistance and the charge transfer resistance of pure $MoSe_2$ and $MoSe_2$/C composites after 5 cycles are larger than that before cycles, this is because the deposition of Li-ions in SEI film increases its thickness after cycles.

Conclusion

In conclusion, we developed a facile solution-phase process to synthesize sheet-like $MoSe_2$/C composites. The as-synthesized $MoSe_2$/C composites were fabricated into Li-ion batteries and exihibited better lithium storage performance, including enhanced cycling stability and rate performance compared to pure $MoSe_2$. The improved electrochemical performance of sheet-like $MoSe_2$/C composites can be attributed to the specially sheet-like microstructure and the presence of carbon embedded in the composites. Typically, the carbon in sheet-like $MoSe_2$/C composites can not only act as a conductive matrix which greatly increases the electrical conductivity and promotes fast electron transportation in the electrode materials, but also maintains structural integrity and hinders the aggregation of nanosheets. Moreover, the composites with sheet-like nanostructure have higher surface area, which provides large effective area for better contact between the electroactives and electrolyte. It is believed that the sheet-like $MoSe_2$/C composites may be promising electrode materials for next-generation LIBs and this approach can also be applied for other transition-metal dichalcogenides.

Acknowledgement

We thanks Prof. Guozhen Shen at Institute of Semiconductors, Chinese Academy of Sciences for helpful discussions.

Notes and references

[a] *Wuhan National Laboratory for Optoelectronics, Huazhong University of Science and Technology, Wuhan 430074, China;*
[b]*School of Mathematics and Physics, University of Science and Technology Beijing, Beijing 100083, China;*
E-mail: chendi@ustb.edu.cn.

1. B. L. Bllis, W. R. M. Makahnouk, Y. Makimura, K. Toghill and L. F. Nazar, Nat. Mater. 2007, 6, 749-753.
2. K. Chang, W. X. Chen, L. Ma, H. Li, F. H. Huang, Z. D. Xu, Q. B. Zhang and J. Y. Lee, J. Mater. Chem., 2011, 21, 6251-6257.
3. L. J. Wang, B. Liu, S. H. Ran, L. M. Wang, L. N. Gao, F. Y. Qu, D. Chen and G. Z. Shen, J. Mater. Chem. A, 2013, 1, 2139-2143.
4. N. Liu, Z. D. Lu, J. Zhao, M. T. McDowell, H. W. Lee, W. T. Zhao and Y. Cui, Nat. nanotechnol. 2014, 9, 187-192.
5. V. Etacheri, R. Marom, R. Elazari, G. Salitra and D. Aurbach, Energy Environ. Sci., 2011, 4, 3243-3262.
6. B. Liu, X. F. Wang, B. Y. Liu, Q. F. Wang, D. S. Tan, W. F. Song, X. J. Hou, D. Chen and G. Z. Shen, Nano Research 2013, 6(7): 525–534.
7. B. Liu, J. Zhang, X. F. Wang, G. Chen, D. Chen, C. W. Zhou and G. Z. Shen, Nano Lett. 2012, 12, 3005 −3011.
8. K. Chang and W. X. Chen, ACS Nano, 2011, 5, 4720-4728.
9. C. Y. Zhao, J. H. Kong, X. Y. Yao, X. S. Tang, Y. L. Dong, S. L. Phua and X. H. Lu, ACS Appl. Mater. Interfaces, 2014, 6, 6392-6398.
10. B. Liu, X. F. Wang, H. T. Chen, Z. R. Wang, D. Chen, Y. B. Cheng, C. W. Zhou and G. Z. Shen, Sci. Rep., 2013, 3, 1622.
11. J. H. Liu and X. W. Liu, Adv. Mater. 2012, 24, 4097-4111.
12. Y. Q. Zhu, H. Z. Guo, H. Z. Zhai, C. B. Cao, ACS Appl. Mater. Interfaces, 2015, 7, 2745−2753.
13. Z. Y. Lu, J. X. Zhu, D. H. Sim, W. W. Zhou, W. H. Shi, H. H. Hng and Q. Y. Yan, Chem. Mater. 2011, 23, 5293 −5295.
14. Y. N. Ko, S. H. Choi, S. B. Park and Y. C. Kang, Nanoscale, 2014, 6, 10511-10515.
15. M. Pumera, Z. Sofer and A. Ambrosi, J. Mater. Chem. A, 2014, 2, 8981-8987.
16. M. S. Wu, Y. H. Qu and Y. P. Lin, J. Electrochem. Soc., 2011, 158 A231-A236.
17. H. Hwang, H. Kim and J. Cho, Nano Lett. 2011, 11, 4826-4830.
18. K. J. Koski and Y. Cui, ACS Nano, 2013, 7, 3739-3743.
19. R. H. Wang, C. H. Xu, J. Sun, Y. Q. Liu, L. Gao, H. L. Yao and C. C. Lin, Nano Energy, 2014, 8, 183-195.
20. J. Z. Wang, L. Lu, M. Lotya, J. N. Coleman, S. L. Chou, H. K. Liu, A. I. Minett and J. Chen, Adv. Energy Mater. 2013, 3, 798–805.
21. U. K. Sen and S. Mitra, ACS Appl. Mater. Interfaces, 2013, 5, 1240−1247.
22. G. D. Du , Z. P. Guo , S. Q. Wang , R. Zeng , Z. X. Chen , H. K. Liu , Chem. Commun.,2010 ,46 , 1106-1108.
23. L. Zhang, X. W. Lou, Chem. Eur. J., 2014, 20, 5219 – 5223.

24. P. L. Sun, W. X. Zhang, X. L. Hu, L. X. Yuan, Y. H. Huang, J. Mater. Chem. A, 2014, 2, 3498–3504.
25. L. Zhang, H. B. Wu, Y. Yan, X. Wang, X. W. Lou, Energy Environ. Sci., 2014, 7, 3302–3306.
26. S. Larentis, B. Fallahazad and E. Tutuc, Appl. Phys. Lett., 2012, 101, 223104.
27. V. Podzorov, M. E. Gershenson, Ch. Kloc, R. Zeis and E. Bucher, Appl. Phys. Lett., 2004, 84, 3301.
28. C. Gong, H. J. Zhang, W. H. Wang, L. J. Colombo, R. M. Wallace and K. Cho, Appl. Phys. Lett., 2013, 103, 053513.
29. C. Tsai, K. Chan, F. A. Pedersen and J. K. Nørskov, Phys. Chem. Chem. Phys., 2014, 16, 13156-13164.
30. L. T. L. Lee, J. He, B. H. Wang, Y. P. Ma, K. Y. Wong, Q. Li, X. D. Xiao and T. Chen, Sci. Rep. , 2014, 4, 4063.
31. Y. F. Shi, C. X. Hua, B. Li, X. P. Fang, C. H. Yao, Y. C. Zhang, Y. S. Hu, Z. X. Wang, L. Q. Chen, D. Y. Zhao and G. D. Stucky, Adv. Funct. Mater. 2013, 23, 1832–1838.
32. H. Tang, K. P. Dou, C. C. Kaun, Q. Kuang and S. H. Yang, J. Mater. Chem. A, 2014, 2, 360–364.
33. L. M. Wang, B. Liu, S. H. Ran, H. T. Huang, X. F. Wang, B. Liang, D. Chen, and G. Z. Shen, J. Mater. Chem., 2012, 22, 23541–23546.
34. C. C. Li, X. M. Yin, L. B. Chen, Q. H. Li and T. H. Wang,Chem.–Eur. J., 2010, 16, 5215–5221.
35. J. Li, L. T. Liu, Y. Liu, M. Z. Li, Y. H. Zhu, H. C. Liu, Y. Kou, J. Z. Zhang, Y. Han and D. Ma, Energy Environ. Sci., 2014, 7, 393–398.
36. X. L. Zhou, J. Jiang, T. Ding, J. J. Zhang, B. C. Pan, J. Zuo and Q. Yang, Nanoscale, 2014, 6, 11046–11051.
37. B. H. Qu, C. Z. Ma, G. Ji, C. H. Xu, J. Xu, Y. S. Meng, T. H. Wang and J. Y. Lee, Adv. Mater. 2014, 26, 3854–3859.
38. X. F. Wang, Q. Y. Xiang, B. Liu, L. J. Wang, T. Luo, D. Chen and G. Z. Shen, Sci. Rep. , 2013, 3, 2007.
39. Y. Wang, G. Z. Xing, Z. J. Han, Y. M. Shi, J. I. Wong, Z. X. Huang, K. Ostrikov, H. Y. Yang, Nanoscale, 2014, 6, 8884–8890.
40. L. Fei, Y. Xu, X. F. Wu, G. Chen, Y. L. Li, B. S. Li, S. G. Deng, S. Smirnov, H. Y. Fan and H. M. Luo, Nanoscale, 2014, 6, 3664–3669.

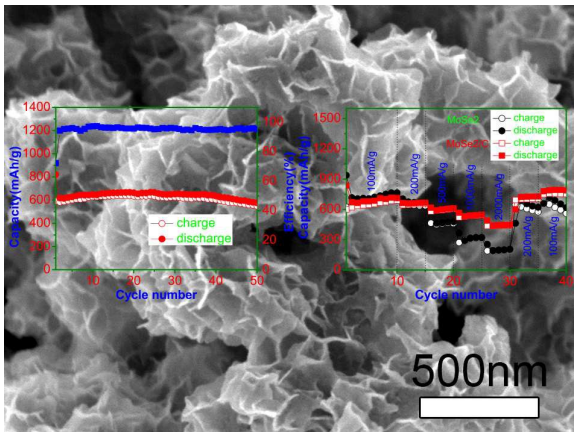

Sheet-like $MoSe_2$/C composites based Li-ion batteries exhibit excellent Li storage performance including high specific capacity, good cyclability and rate capability.